ELSEVIER

Surface Science 418 (1998) 395–406

surface science

Solution of Ge(111)-(4 × 4)-Ag structure using direct methods applied to X-ray diffraction data

C. Collazo-Davila [a,*], D. Grozea [a], L.D. Marks [a], R. Feidenhans'l [b], M. Nielsen [b], L. Seehofer [c], L. Lottermoser [c], G. Falkenberg [c], R.L. Johnson [c], M. Göthelid [d], U. Karlsson [d]

[a] *Department of Materials Science, Northwestern University, Evanston, IL 60208, USA*
[b] *Condensed Matter Physics and Chemistry Department, Risø National Laboratory, 4000 Roskilde, Denmark*
[c] *II. Institut für Experimentalphysik, Universität Hamburg, Luruper Chaussee 149, 22761 Hamburg, Germany*
[d] *Department of Physics, Materials Physics, Royal Institute of Technology, 10044 Stockholm, Sweden*

Received 7 April 1998; accepted for publication 13 August 1998

Abstract

A structure model for the Ge(111)-(4 × 4)-Ag surface is proposed. The model was derived by applying direct methods to surface X-ray diffraction data. It is a missing top layer reconstruction with six Ag atoms placed on Ge substitutional sites in one triangular subunit of the surface unit cell. A ring-like assembly containing nine Ge atoms is found in the other triangular subunit. The stability of the ring assembly may be due to Ge–Ge double bond formation. Trimers of Ge atoms, similar to the trimers found on the Ge(111)-($\sqrt{3}\times\sqrt{3}$)R30°-Ag surface, are placed in the corners of the unit cell.

Keywords: Computer simulations; Direct methods; Ge(111)-(4 × 4)-Ag; Germanium; Silver; Surface relaxation and reconstruction; Transmission high-energy electron diffraction; X-ray scattering, diffraction and reflection

1. Introduction

Over the last decade there has been a great effort trying to understand the atomic geometry of metal-induced reconstructions on elemental semiconductor surfaces. An example of such a system is Ag on the Ge(111) surface. At low coverages ca 0.3 monolayers (ML), (4 × 4) and (3 × 1) structures are formed. Around 1 ML a ($\sqrt{3}\times\sqrt{3}$)R30° structure appears, and finally at coverages >1 ML the ($\sqrt{3}\times\sqrt{3}$)R30° structure transforms into a (6 × 6) reconstruction [1]. Of these four structures, only the ($\sqrt{3}\times\sqrt{3}$)R30° is known. It has the honeycomb-chained trimer (HCT) structure [2–4], where the top layer of Ge-atoms are missing and the remaining Ge-atoms in the outermost bilayer form trimers which are surrounded by Ag atoms, is similar to the structure of the Si(111)-($\sqrt{3}\times\sqrt{3}$)R30°-Ag surface [5,6]. The (3 × 1) reconstruction has only been seen as small insets between (4 × 4) domains and domains of the native Ge(111)-c(2 × 8) reconstruction. Its structure may be similar to the Si(111)-(3 × 1)-Ag structure [7,8,19] which was solved very recently [10–12].

In this paper we will focus on the (4 × 4) structure. This structure has been studied primarily by

* Corresponding author. Fax: +1 847 4917820.

0039-6028/98/$ – see front matter
PII: S0039-6028(98)00664-5

scanning tunneling microscopy (STM) and photoelectron spectroscopy, but little is known about the atomic geometry. The coverage of Ag has been determined to be around 0.3 ML [13], and high resolution core level photoelectron spectroscopy shows that all Ag atoms sit in nearly the same site [3]. Furthermore, the binding energy of the Ag atoms does not change as the $(\sqrt{3}\times\sqrt{3})R30^\circ$ reconstruction is formed, suggesting that the Ag site in the two structures is similar [3]. STM images show that the unit cell is composed of two triangular subunits with widely varying images depending on the tip bias [4,8,9,14]. While imaging the filled states, six protrusions are seen in one of the triangular subunits. A comparison with neighboring $c(2\times8)$ domains reveals that the protrusions are located in top sites of the underlying Ge lattice. This is an unusual site, and suggests a (at least partial) missing top layer (MTL) type of reconstruction, which would agree with STM studies of the terrace heights between neighboring (4×4) and $(\sqrt{3}\times\sqrt{3})R30^\circ$ domains [9]. The empty state images display three protrusions in the other triangular subunit which have been attributed to three Ge adatoms, similar to the adatoms on the $c(2\times8)$ surface. However, the (4×4) unit cell is large which hampers structural verification. In fact, it was impossible to verify the structure with a strong crystallographic tool like surface X-ray diffraction, and it was not possible to suggest an alternative structure [3,15].

In a diffraction experiment only the amplitudes and not the phases of the reflections are determined, and this prevents a direct Fourier inversion of the data. With the measured amplitudes alone, contours plots of the Patterson function can be obtained providing interatomic vector information, which in the present case was not sufficient to make a valid trial structure [15]. Phasing of structure factors, known as direct methods [16], has been used for many years in conventional three-dimensional bulk crystallography. Recently, direct methods have been successfully applied to two-dimensional X-ray diffraction and transmission electron diffraction data sets [10,17–23]. In this paper, we applied these methods on X-ray diffraction data obtained previously on the Ge(111)-(4×4)-Ag surface [15]. This allowed us to solve the structure. The basic ingredients in the structure are the six Ag atoms situated in a MTL reconstruction in one half of the unit cell. Ge trimers, similar to the Ge-trimers at the $(\sqrt{3}\times\sqrt{3})R30^\circ$ structure are found in the corners of the unit cell. The Ag free part of the unit cell shows a major restructuring of the Ge bilayer.

2. Experimental

The Ge(111) crystals were cleaned by repeated cycles of sputtering and annealing at 650°C for a few minutes until a sharp $c(2\times8)$ low energy electron diffraction (LEED) pattern was obtained. Silver was deposited from a Knudsen cell onto the sample at 400°C. The surface was inspected by LEED and reflection high energy electron diffraction (RHEED) to verify that a uniform (4×4) structure was present on the surface. Furthermore, the surfaces were thoroughly examined by STM in order to assure the existence of a highly ordered structure. The STM images were similar to previous images from the literature. The sample was thereafter transferred into a portable ultrahigh vacuum (UHV) chamber that was mounted on the X-ray diffractometer.

Two sets of X-ray diffraction data were measured. The first set was taken at the wiggler beamline W1 at the Hamburger Synchrotron Radiation laboratory (HASYLAB) at an X-ray wavelength of 1.40 Å. The sample was aligned on the optical surface such that the angle of incidence was kept constant throughout the measurements. In order to maximize the intensity, the angle of incidence was set to the angle for total external reflection [24]. The active area on the sample was defined by a 1 mm slit in front of the sample and a 1.5 mm slit on the detector arm directly after the sample. A position sensitive detector with a 0.6° acceptance angle in the surface plane and 2.8° perpendicular to that plane was used to measure the intensities of the reflections. Integrated intensities were measured by rocking scans (ω-scans) around the surface normal. A total of 107 integrated intensities of in-plane, fractional-order reflections were

obtained. The structure factor intensities were obtained by correcting the measured intensities with a Lorentz factor, for variations in the active area [24]. The intensities were averaged by symmetry to obtain a set of 64 structure factor intensities from non-equivalent reflections. The uncertainties were estimated from the reproducibility between the strong symmetry-equivalent reflections. The reproducibility was about 13%. The second data set was taken at beamline BW2 using an X-ray wavelength of 1.24 Å. Here a total of 112 integrated intensities of in-plane, fractional order reflections were obtained, out of which 71 were non-equivalent. The reflections are indexed with respect to the (4×4) surface unit.

3. Analysis

As mentioned above, the traditional approach based on finding the interatomic vectors in the contour map of the Patterson function does not provide a useful route for structure determination. Instead we used direct methods. Direct methods exploit probability relationships which exist between the amplitudes and the phases of the diffracted beams to solve the diffraction phase problem. For example, if the phases of two reflections, $\boldsymbol{h}_1$ and $\boldsymbol{h}_2$, are known, then the phase of the reflection $\boldsymbol{h}_3=\boldsymbol{h}_1+\boldsymbol{h}_2$ can be estimated with a measurable degree of certainty. The degree of certainty for the estimated phase of $\boldsymbol{h}_3$ increases with the amplitudes of the three reflections, $\boldsymbol{h}_1$, $\boldsymbol{h}_2$ and $\boldsymbol{h}_3$. In practice, one starts with a basis of a few strong beams with assigned phases and estimates the phases of new beams. An iterative procedure is set up in which phase estimates are eventually assigned to all measured amplitudes. A figure of merit is then calculated for the complete set of phases and amplitudes to quantify the degree to which the probability relationships are satisfied. Each new basis set one begins with can lead to a distinct final set of phases with its own figure of merit. By searching through all of the possible starting basis sets (e.g. in a grid pattern, randomly, or with a global optimization algorithm) one can pick out the final sets of phases giving the lowest figures of merit. Only those solution sets with the lowest figures of merit are used to create maps of the electron density through inverse Fourier transforms of the measured amplitudes. For an introduction to modern direct methods the reader is referred to Ref. [16]. The details of the phasing procedure adapted to two dimensional surface data (as in this study) have been described elsewhere [17,18], and a brief description of the unique features of the approach we use is given in Appendix A.

Before one can apply direct methods to diffraction data, an assumption about the unknown structure's symmetry must be made. STM images from the Ge(111)-(4×4)-Ag surface [4,8,9,14] belong to the p3m1 plane group. While slight deviations from p3m1 symmetry could go undetected by STM, the deviations would have to be minor and would not significantly alter the phasing results. The 14 beams forming the previously mentioned basis set for the phasing analysis are shown in Table 1 along with their measured amplitudes and the limits placed on their phases for each of the two data sets. With p3m1 symmetry, beams

Table 1
Reflections forming the basis set for the phasing analysis

(h, k)	$\lvert F\rvert$ Set 1	$\lvert F\rvert$ Set 2	Phase (°)
(7, 7)	1.96	2.15	360
(5, 2)	3.23	3.23	180–360
(4, 3)	2.82	2.82	30–120
(7, 1)	1.29	1.38	45–360
(5, 3)	2.11	1.62	45–360
(7, 0)	1.94	2.12	45–360
(8, 3)	0.89	1.22	45–360
(6, 1)	0.81	1.14	45–360
(4, 2)	1.51	1.19	45–360
(7, 5)	0.84	0.76	45–360
(11, 1)	1.59	1.64	45–360
(7, 3)	0.72	0.80	45–360
(8, 2)	0.85	0.72	45–360
(11, 2)	0.69	0.46	45–360

The measured amplitudes for the second data set have been scaled to the first, and their absolute magnitudes are arbitrary. The phase of (7, 7) was fixed at 360° through sigma-1 relationships. The phases of all other reflections were varied within the ranges shown. The limits on (5, 2) and (4, 3) were used to define an orgin and to select an enantiomorph.The phases of (5, 2) and (4, 3) were varied in steps of 60° and 30°, respectively, while all other phases were varied in steps of 45°.

belonging to the class of reflections (n, n), where n is any integer, have a phase of either 0° or 180°. Based on sigma-1 relationships [25] with the (4, 3) and (5, 2) beams, the (7, 7) beam was assigned a phase of 0°. Origin definition and enantiomorph selection were achieved by restricting the ranges of the phases of the (4, 3) and the (5, 2) reflections. The phases of the beams in the basis set were globally searched using a genetic algorithm optimized to find different local minima, each corresponding to a plausible solution with a low figure of merit [18].

The 20 best sets of phases (giving the lowest figures of merit at the end of the phasing process) were used to generate electron density maps. All of the maps showed the same basic structure with only minor variations. Fig. 1 shows typical maps for each data set. Since the data used in this study were purely two-dimensional, the electron density maps are projections of the (4×4) structure onto a plane parallel to the Ge surface. The position of atomic sites in the direction normal to the Ge surface must be inferred from bond length arguments. While the relative intensities of the peaks seen in Fig. 1 changed from map to map within the top 20 phasing solutions, the positions of the peaks were always the same. The site arrowed in Fig. 1 was more prominent in maps from the second data set and failed to appear at all in some maps from the first data set. The two possibilities that this site could be either partially occupied or an artifact due to noise in the data were both considered in the subsequent analysis. However, each non-arrowed site in Fig. 1 appeared in all 20 maps and was considered to correspond to either a Ge or a Ag atom site.

To determine which of the sites revealed through the phasing analysis correspond to Ge atoms and which to Ag, we used the conventional method of comparing the measured diffraction intensities with intensities kinematically simulated from possible models. Allowing for a silver coverage between 1/4 and 5/8 ML we considered models with four and ten sites in each unit cell occupied by Ag atoms and the remaining sites filled with Ge. The agreement between the measured and simulated intensities was quantified using two different parameters for each model. We used a standard

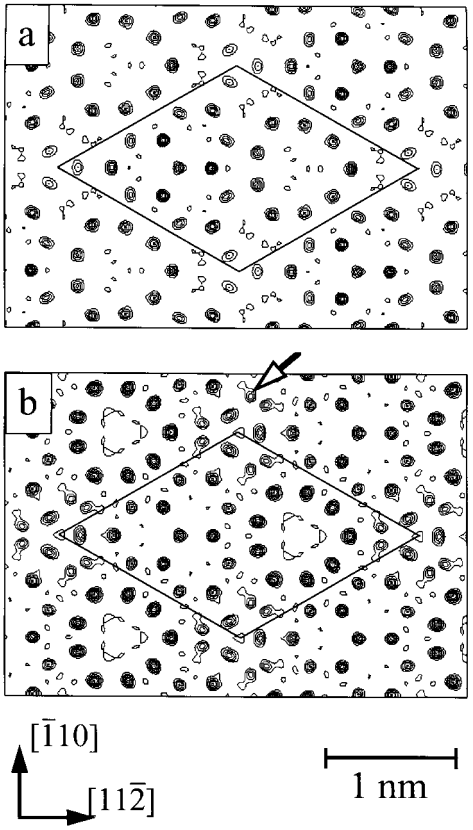

Fig. 1. Contour map of the calculated electron density using phases estimated through direct methods for (a) data set 1 and (b) data set 2. For each map six contour levels were evenly spaced between zero and the maximum electron density. The arrow in (b) indicates a partially occupied Ag site which has a lower occupancy for the first data set.

R-factor defined as:

$$R\equiv\frac{\sum_{j=1}^{N}|I_j^{\mathrm{meas}}-I_j^{\mathrm{calc}}|}{\sum_{j=1}^{N}I_j^{\mathrm{meas}}} \tag{1}$$

where I^{meas} is a measured intensity, I^{calc} is the simulated intensity, and N is the total number of measured reflections. Also a reduced χ value was calculated:

$$\chi\equiv\frac{1}{N-M}\sum_{j=1}^{N}\frac{|I_j^{\mathrm{meas}}-I_j^{\mathrm{calc}}|}{\sigma_j} \tag{2}$$

where M is the number of variables in the refine-

ment and σ_j is the uncertainty in the jth measured intensity. Refinements using the R-factor are insensitive to the weaker reflections in a data set since the weak reflections do not contribute significantly to the sums in Eq. (1). Therefore, in an R-factor fit the largest measured intensities will match the simulated intensities within unrealistically small percentage errors at the expense of a reasonable match for the weakest reflections. The χ value provides a more appealing distribution of fitting errors by normalizing each term in the sum by an estimated error. All of the refinements discussed in this paper were done twice – once employing a χ value and once using an R-factor. While the numbers listed in the tables and used to make the figures are exclusively from the χ refinements, we quote the R-factor along with the χ value obtained from each model for reference, since the R-factor is a widely used test. We favor the χ value over the more common χ^2 value because it is a more robust measure of agreement less sensitive to deviations from the ideal situation of perfectly gaussian-distributed measurement errors.

As an initial refinement step we did not place any atoms at the site which is arrowed in Fig. 1, and we compared the simulated intensities only with the first data set for which the arrowed site was not prominent. Assuming that all of the phasing analysis sites represent atoms in the top surface layer, we also added a complete double layer of Ge atoms to each model to simulate relaxations extending into the bulk. Accordingly, the three possible registries between the surface layer and the relaxed bulk double layer were investigated for each different distribution of Ge and Ag atoms among the surface sites. All refinements of the atom positions were done within the p3m1 plane group. Two Debye–Waller factors were included in the refinement, one for the surface Ge and one for the Ag. The Debye–Waller factor for the relaxed double layer was set at the value for bulk Ge. Under these conditions, the best fit to the measured intensities was obtained with the model shown in Fig. 2 which yielded $\chi=2.31$ and $R=0.21$. Counting a scaling term, 21 variables were used in this fit for the 71 measured reflections in data set 1.

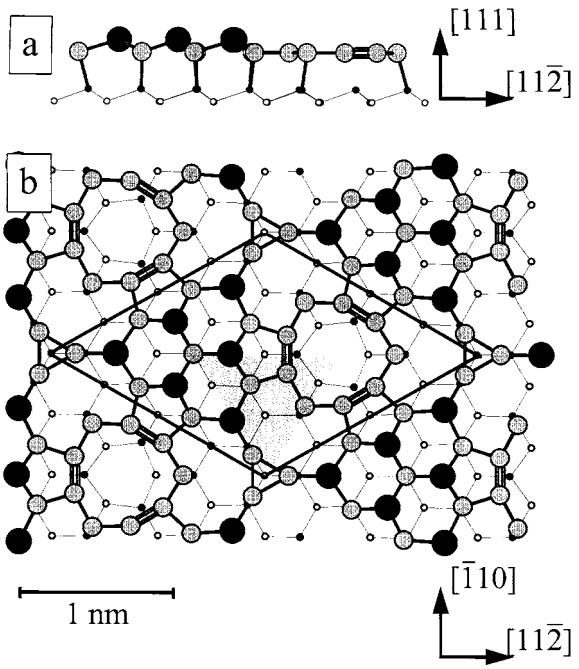

Fig. 2. Proposed model for the Ge(111)-(4×4)-Ag surface. (a) Side view showing only those atoms which are contained within the (4×4) unit cell cell ($a=b=16.002$ Å, $\gamma=120°$) which is outlined in (b), the top view. Large black circles represent Ag, and everything else is Ge. The double lines between Ge atoms in the right half of the unit cell represent double bonds which are explained in Section 4. The asymmetric unit for the plane group p3m1 is shaded in gray.

The simulated diffraction intensities are very sensitive to the number and location of surface atoms, so the basic structure seen in Fig. 2 (ignoring distinctions between Ag and Ge atoms) can be accepted with a high degree of confidence. However, the atomic numbers of Ag and Ge are not too far apart (47 and 32, respectively), so the diffraction data in this study afford relatively weak sensitivity to chemical species. For example, a model in which the six nearest surface sites surrounding the trimers at the corners of the (4×4) unit cell are filled by Ag rather than Ge will refine to a χ value of 2.91 and an R-factor of 0.23. Other distributions of Ag and Ge among the same surface sites yield χ values and R-factors which are only slightly higher. Nevertheless, we can state that the positions of the atoms in this surface structure have been uniquely determined. In addition, the

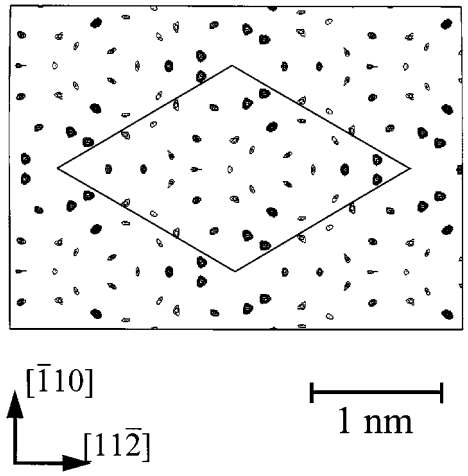

Fig. 3. Fourier difference map calculated for the second data set using the model shown in Fig. 2. Six contour levels were evenly spaced between half the maximum and the maximum electron density to highlight the strongest peaks.

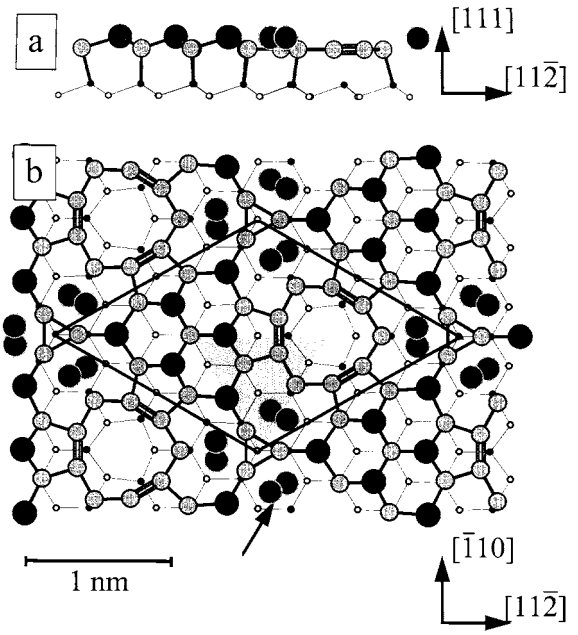

Fig. 4. The proposed (4×4) model structure with a partially occupied Ag site shown by large dark-gray circles (arrowed). The occupancy of this site was refined to 0.27 and 0.36 for data sets 1 and 2, respectively. (a) Side view showing only those atoms which are contained within the (4×4) unit cell cell which is outlined in (b), the top view. Large black circles represent Ag, and everything else is Ge. The double lines between Ge atoms in the right half of the unit cell represent double bonds. The asymmetric unit for the plane group p3m1 is shaded in gray.

distribution of Ag atoms shown in Fig. 2 is consistent with all of the experimental data available on submonolayer coverages of Ag on Ge(111) as will be expanded upon in Section 4.

The model shown in Fig. 2 was also refined using the measured intensities from the second data set. While the atom positions did not significantly change (the largest shift was 0.17 Å), the fit was not as good for the second data set with $\chi=3.26$ and $R=0.29$. To look for additional atom sites, a Fourier difference map was created and is shown in Fig. 3. A strong peak in the difference map is seen at the location corresponding to the arrowed site in Fig. 1. This suggests that the arrowed site is not an artifact and is likely due to a partially occupied Ag site which has a higher occupancy for the second data set. The other strong peak seen in Fig. 3 is located slightly displaced from a site already occupied by Ge. We investigated the possibility that this site was Ag instead of Ge, but a better fit to the intensities was not obtained.

Working with the hypothesis that the Ge(111)-(4×4)-Ag structure can accommodate a variable range of Ag through a partially occupied site, we refined a new model with the second data set (Fig. 4). The new model contained four new variables: an x and a y position for the new partially occupied Ag site, a variable for the occupancy of the site, and a Debye–Waller factor for the site. A better fit was obtained with $\chi=2.63$ and $R=0.13$ at an occupancy of 0.3 for the new Ag site. Using the new model for the first data set yielded $\chi=2.15$ and $R=0.14$ with an occupancy of 0.2 for the Ag site. Finally, we fit both data sets together with a single set of values for all of the atomic positions and Debye–Waller factors. A separate occupancy for the partial Ag site was refined for each data set. In the final fit, the occupancies refined to 0.27 and 0.36 for the first and second data sets respectively yielding $\chi=2.22$ and $R=0.18$. The atomic positions and Debye–Waller factors for this fit are shown in Table 2. With a separate scaling factor for each data set, 28 parameters were varied, and including both data sets gave a total of 137 meas-

Table 2
Atom positions for the model in terms of a (4×4) unit cell in the p3m1 plane group: $a=b=16.002$ Å, $\gamma=120^\circ$

Atom	x	x (unrelaxed)	y	y (unrelaxed)	Wyckoff	z
Ag	0.4197	–	0.5803	–	d	Surface
Ag	0.1511	–	0.3021	–	d	Surface
Ag	0.2099	–	0.1444	–	e	Surface
Ge	0.0563	–	0.1125	–	d	Surface
Ge	0.3826	–	0.1913	–	d	Surface
Ge	0.4774	–	0.3706	–	e	Surface
Ge	0.3436	–	0.4102	–	e	Surface
Ge	0.3333	–	0.6667	–	b	Surface
Ge	0.3349	0.3333	0.1674	0.1667	d	Layer 1
Ge	0.5772	0.5833	0.4228	0.4167	d	Layer 1
Ge	0.0793	0.0833	0.1586	0.1667	d	Layer 1
Ge	0.3272	0.3333	0.4074	0.4167	e	Layer 1
Ge	0.3333	0.3333	0.6667	0.6667	b	Layer 1
Ge	0.2475	0.2500	0.4951	0.5000	d	Layer 2
Ge	0.5102	0.5000	0.2551	0.2500	d	Layer 2
Ge	0.5012	0.5000	0.4988	0.5000	d	Layer 2
Ge	0.2512	0.2500	0.2474	0.2500	e	Layer 2
Ge	0.0000	0.0000	0.0000	0.0000	a	Layer 2

The Wyckoff letter corresponds to the site symmetry. A Wyckoff letter of "d" indicates a site on a mirror plane and therefore the x and y positions are symmetry related and only one variable is used to describe the atom position. "e" is a general site and so both the x and the y values are independently refined varibles."a" and "b" are fixed sites lying on a three-fold axis and are not refined. The occupancy of the partial Ag site was fit with 0.27 for data set 1 and 0.36 for data set 2. Isotropic Debye–Waller factors (defined as $B=8\pi^2\langle u^2\rangle$, where $\langle u^2\rangle$ is the mean square atomic displacement) were fit at 6.60 Å^2 for fully occupied Ag, 3.14 Å^2 for partially occupied Ag, 3.74 Å^2 for Ge in the surface layer, and 0.84 Å^2 for Ge in layers 1 and 2. (In pure bulk samples at 280 K, $B=0.70$ Å^2 for Ag and $B=0.57$Å^2 for Ge [26].)

urements. Fourier difference maps created from this final model for both data sets were essentially featureless with no well-resolved peaks.

4. Discussion

Three main features of the Ge(111)-(4×4)-Ag structure will be reviewed in this section: similarities to the Ge(111)-$(\sqrt{3}\times\sqrt{3})$R30°-Ag surface, similarities to the Ge(111)-(3×1)-Ag surface, and the nature of the partially occupied Ag site.

Weitering and Carpinelli have already noted strong indications that the (4×4) and the $(\sqrt{3}\times\sqrt{3})$R30° reconstructions induced by Ag on Ge(111) are related [9]. The structure for the Ge(111)-$(\sqrt{3}\times\sqrt{3})$R30°-Ag surface, the honeycomb-chained-trimer structure [2–4], is illustrated in Fig. 5. It consists of an array of Ge trimers, with each trimer surrounded by six Ag atoms. Consequently, Weitering and Carpinelli suggested that the Ge trimer serves as a common building block for the (4×4) structure as well. Our proposed model supports this view. The Ge trimer with the three nearest neighboring Ag atoms found at the corners of the unit cell in Fig. 2 matches the basic structural unit of the $(\sqrt{3}\times\sqrt{3})$R30° surface. The model is also in agreement with the high resolution core level photoelectron spectroscopy results which suggested that all of the Ag atom are in nearly identical sites, in both the (4×4) and the $(\sqrt{3}\times\sqrt{3})$R30° structures [3]. The Ag coverage for the proposed (4×4) model is 3/8 ML while the coverage for the $(\sqrt{3}\times\sqrt{3})$R30° surface is 1 ML. The comparison of Fig. 2 with Fig. 5 reveals an easy path of transformation from the (4×4) structure to the $(\sqrt{3}\times\sqrt{3})$R30° surface upon the addition of 5/8 ML of Ag [or 10 Ag atoms per (4×4) unit cell]. All that is required in each unit cell is the removal of three Ge atoms and the addition of the ten Ag atoms. The six Ag atoms

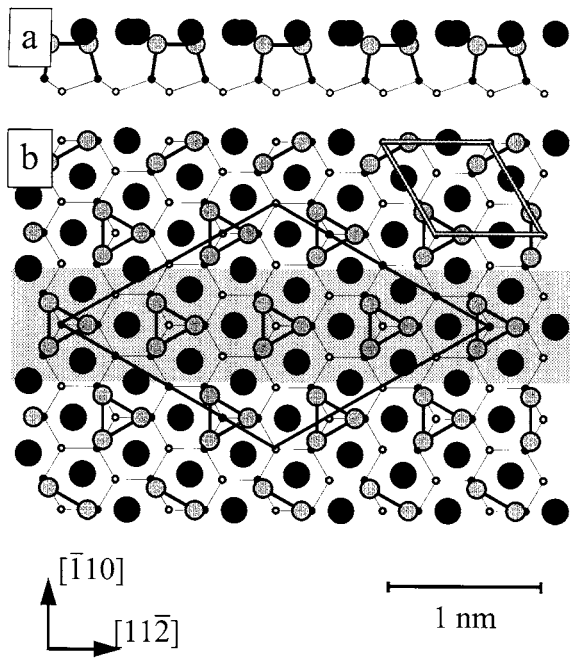

Fig. 5. Honeycomb-chained-trimer model for the Ge(111)-($\sqrt{3}\times\sqrt{3}$)R30°-Ag surface. (a) Side view, (b) top view. For clarity, the side view shows only those atoms contained within the gray-shaded region of (b). Large black circles represent Ag, and everything else is Ge. A (4×4) unit cell has been outlined in black to facilitate comparison with Figs. 2 and 4. The ($\sqrt{3}\times\sqrt{3}$)R30° unit cell is outlined in gray and white in the top right corner of (b).

already in the (4×4) unit cell only need to be slightly displaced, and apart from the removal of the three Ge atoms, the bonds between the surface layer Ge and the first bulk double layer remain intact.

One might also suspect that the (4×4) structure is related to the (3×1) structure since the (3×1) structure occurs at only a slightly lower Ag coverage (1/3 ML), and small domains of (3×1) have often been observed at the edges of (4×4) domains [4,8,9]. In fact, based on recent first-principles calculations [27], a link can be drawn between the Ge(111)-(3×1)-Ag surface and the nine member Ge ring in the Ge(111)-(4×4)-Ag structure. The common feature is the formation of a Ge–Ge double bond which has been suggested to be part of the (3×1) structure by Erwin and Weitering [27]. Fig. 6 illustrates this point by highlighting a fragment of the Ge ring in the (4×4) structure which has a similar local geometry to the basic (3×1) structure. If we assume that a double bond forms at the location shown in Fig. 6, then we eliminate all of the dangling bonds on the nine Ge atoms making up the ring, and we can qualitatively understand the stability of this unique surface structure.

The partially occupied Ag site included in our final model suggests two possibilities. First, the Ge(111)-(4×4)-Ag surface phase may actually be a surface solution stable over a range of Ag coverages at room temperature, as has been reported for the Si(111)-($\sqrt{3}\times\sqrt{3}$)R30°-Au phase [28]. As seen in Fig. 4, the six positions per unit cell for the partially occupied site can be grouped into three pairs. The two positions in a pair are too close to both be occupied at the same time, so the maximum possible occupancy is 0.5, which would give an upper coverage boundary for the (4×4) phase of 0.5625 ML. The lower coverage boundary for the phase would be 0.375 ML corresponding to an occupancy of zero (the structure in Fig. 2). Alternatively, the Ge(111)-(4×4)-Ag phase with the partial occupancy site may be a metastable surface solution at room temperature which, if given enough thermal energy to overcome an activation barrier, would phase separate into either ($\sqrt{3}\times\sqrt{3}$)R30° plus (3×1) domains or into ($\sqrt{3}\times\sqrt{3}$)R30° plus "basic" (4×4) domains without the partially occupied Ag site. In either case, the basic Ge(111)-(4×4)-Ag structure is that shown in Fig. 2 without the partially occupied site, and more studies including the effects of annealing on the reconstructions would be required to determine a surface phase diagram for this system.

The random site occupancy disorder for the partially occupied site discussed above would give rise to a diffuse background in diffraction experiments. Transmission electron diffraction data from surfaces with regions of (4×4) mixed with regions of ($\sqrt{3}\times\sqrt{3}$)R30° indicate an additional type of disorder giving rise to structured diffuse scattering. Fig. 7 shows two diffraction patterns: the first from a region that is predominantly covered by the (4×4) structure and the second from a region in

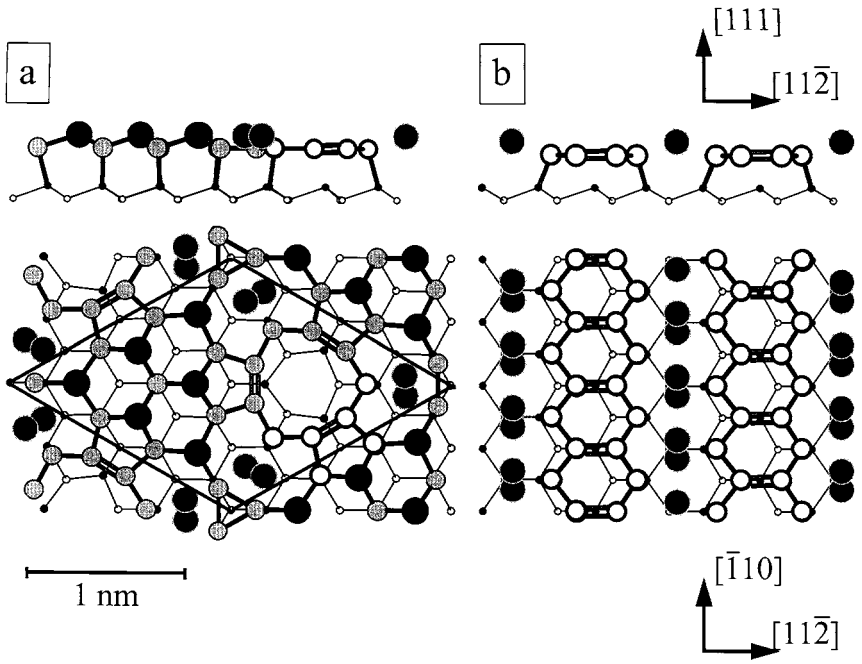

Fig. 6. A comparison of (a) Ge(111)-(4×4)-Ag and (b) Ge(111)-(3×1)-Ag. Large black circles represent Ag, large dark-gray circles represent partially occupied Ag, and everything else is Ge. In (a) five Ge atoms are shown in white to highlight a structure fragment which is similar to the basic Ge(111)-(3×1)-Ag structure. The double lines between the Ge atoms represent double bonds. The side view in (a) shows only those atoms contained within the (4×4) unit cell which is outlined in the top view.

which the (4×4) and $(\sqrt{3}\times\sqrt{3})$R30° structures coexist. In the second diffraction pattern, diffuse rings surround the strongest $(\sqrt{3}\times\sqrt{3})$R30° spots. These rings are remarkably similar to the diffuse scattering reported on the Au/Si(111) surface during the transformation between the Si(111)-$(\sqrt{3}\times\sqrt{3})$R30°-Au and the Si(111)-(6×6)-Au structures [29–34]. In the Au/Si(111) case the rings can be attributed to a rotationally disordered yet evenly-spaced array of domain walls separating regions of local $(\sqrt{3}\times\sqrt{3})$R30° order. In the case of Ag/Ge(111) the situation may be similar with evenly-spaced boundaries forming between the $(\sqrt{3}\times\sqrt{3})$R30° and the (4×4) domains.

5. Conclusion

By applying direct methods to surface X-ray scattering data, we have solved the Ge(111)-(4×4)-Ag structure. The structure is a MTL reconstruction with six Ag atoms placed on Ge substitutional sites in a triangular subunit of the unit cell. In the other triangular subunit a ring-like assembly of nine Ge atoms is formed. The presence of three double bonds similar to those found on the Ge(111)-(3×1)-Ag surface could explain the stability of the nine-member Ge ring. Trimers of Ge atoms are found at the corners of the (4×4) unit cell. Fractionally occupied Ag sites suggest either a solid surface solution or a possible first step in the transformation from the (4×4) structure to the $(\sqrt{3}\times\sqrt{3})$R30° structure as a function of increasing Ag coverage. The structure is in very good agreement with STM measurements [4,8,9,14] and high resolution core level photoelectron spectroscopy [3].

Acknowledgements

The authors thank the staff of HASYLAB for their help and assistance throughout the measure-

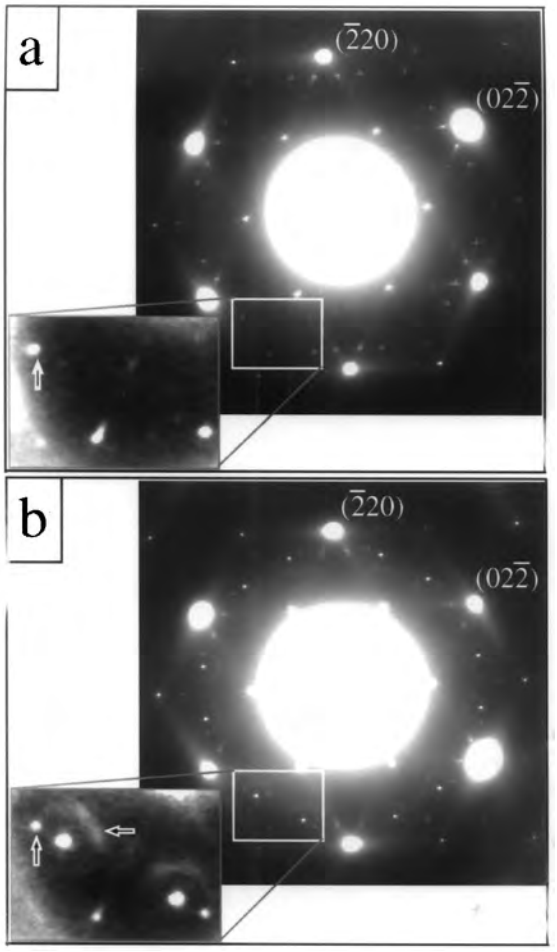

Fig. 7. Transmission electron diffraction patterns taken close to Ge(111) zone-axis. (a) From a region covered by the (4×4) structure. (b) From a region with both (4×4) and $(\sqrt{3}\times\sqrt{3})R30^\circ$ domains. The magnified region in (b) shows diffuse rings (horizontal arrow) surrounding the most intense $(\sqrt{3}\times\sqrt{3})R30^\circ$ spots. The diffuse rings are not present in (a). The vertical arrows point to the same (4×4) surface reflection in both (a) and (b).

ments. They also thank E. Landemark, D.-M. Smilgies, M. Foss and C. Klink for participating in X-ray scattering measurements. The work was supported by the Danish National Research Council through Dansync. CC, DG and LDM acknowledge the support of the National Science Foundation through Grant No. DMR-9214505.

Appendix A

Minimum relative entropy/Kullback–Leibler distance

In our implementation of direct phasing methods for two-dimensional data, we use unitary structure factors [16] and an iterative algorithm which minimizes the relative entropy [17,18]. While "Maximum Entropy" has been used in a crystallographic environment, we are not aware of the use of the relative entropy or Kullback–Leibler distance [35] [also known as cross entropy, information divergence and information for discrimination (see Ref. [36] for a much more detailed analysis)] so a little clarification is appropriate. Considering the standard definition of entropy or self-information (in real space $\boldsymbol{r}$) as:

$$S=-\Sigma\rho(\boldsymbol{r})\ln\rho(\boldsymbol{r});\ \text{with}\ \Sigma\rho(\boldsymbol{r})=1 \tag{A1}$$

$$S=-\Sigma\left[\rho(\boldsymbol{r})\ln\left\{\frac{\rho(\boldsymbol{r})}{e\langle\rho(\boldsymbol{r})\rangle}\right\}+\langle\rho(\boldsymbol{r})\rangle\right] -\Sigma\rho(\boldsymbol{r})\ln\{e\langle\rho(\boldsymbol{r})\rangle\}+1 \tag{A2}$$

$$=-\Sigma\left[\rho(\boldsymbol{r})\ln\left\{\frac{\rho(\boldsymbol{r})}{e\langle\rho(\boldsymbol{r})\rangle}\right\}+\langle\rho(\boldsymbol{r})\rangle\right]-\ln\{\langle\rho(\boldsymbol{r})\rangle\} \tag{A3}$$

The relative entropy is the negative of the first term in Eq. (A3), and maximizing the conventional entropy is thus equivalent to minimizing the relative entropy. More usefully, the relative entropy as defined above is a metric of the deviation of the distribution $\rho(\mathbf{r})$ from flat, and can be used as such. The figure of merit (FOM) used to gauge the plausibility of a particular phasing solution is defined as:

$$\mathrm{FOM}=\frac{\sum_{\boldsymbol{k}}|U_n(\boldsymbol{k})-\beta U_{n+1}(\boldsymbol{k})|}{\sum_{\boldsymbol{k}}|U_n(\boldsymbol{k})|} \tag{A4}$$

where n is the phasing iteration step number, β is a scaling term calculated to minimize the sum in the numerator, $U(\boldsymbol{k})$ is the unitary structure factor for the reflection $\boldsymbol{k}$, and the sums are taken over all reflections except $\boldsymbol{k}=0$. This FOM is the pro-

jection of the relative entropy onto the set of measured reflections in reciprocal space.

To strengthen the algorithm further, we modify the unitary structure factors in reciprocal space by a "window function" $W(\boldsymbol{k})$, using $U'(\boldsymbol{k})$ where:

$$U'(\boldsymbol{k}) = W(\boldsymbol{k})U(\boldsymbol{k}) \tag{A5}$$

The window function (in real space) is defined to be an eigensolution of the "relative entropy sharpening operator" $\hat{\mathbf{O}}$ via the equation

$$A(\boldsymbol{r})^*\hat{\mathrm{O}}w(\boldsymbol{r}) = A(\boldsymbol{r})^*\left\{w(\boldsymbol{r})\ln\left(\frac{w(\boldsymbol{r})}{\langle w(\boldsymbol{r})\rangle}\right)\right\} = \lambda A(\boldsymbol{r})^* w(\boldsymbol{r}) \tag{A6}$$

in which * is convolution, and $A(\mathbf{r})$ is the Fourier transform of an aperture function surrounding the set of measured reflections. For a set of identical non-overlapping atoms, with kinematical diffraction, the relative entropy defined in this way is identically zero for the true solution – we have built in a pattern recognition component. As such the FOM is the log-likelihood (p. 18 of Ref. [36]) of the error in the hypothesis that a given solution corresponds to a set of atoms.

There are *very strong* similarities to the Gerchberg–Saxton [37] and Fienup [38,39] algorithms, as well as the Sayre equation [40], with the relative entropy sharpening operator applying a self-consistent (for atoms) constraint on the solutions with a self-consistency FOM. The construction:

$$u_{n+1}(\boldsymbol{r}) = u_n(\boldsymbol{r})\ln\left\{\frac{u_n(\boldsymbol{r})}{\langle u_n(\boldsymbol{r})\rangle}\right\} \tag{A7}$$

is a first-order iterative solution for zeros of the relative entropy used in a Tangent-formula update scheme; since we only want approximate solutions a primitive search is appropriate. (The radius of convergence of the iterative scheme is finite, so a search over initial starting phases is required.)

The method has strong similarities to crystallographic Maximum Entropy approaches, for instance strong non-linearities with the ability to interpolate unmeasured reflections. Rather than a precise numerical optimization of the (absolute) entropy and weak constraints on the moduli of the structure factors, a loose optimization is used via the iteration [Eq. (A7)], with tight constraints on the structure factors. The avoidance of any gradient search for entropy maximization both simplifies and increases the numerical speed.

References

[1] G. Le Lay, Surf. Sci. 132 (1983) 169.
[2] H. Huang, H. Over, S.Y. Tong, J. Quinn, F. Jona, Phys. Rev. B 49 (1994) 13483.
[3] M. Göthelid, M. Hammar, U.O. Karlsson, C. Wigren and, G. Le Lay, Phys. Rev. B 52 (1995) 14104.
[4] D.J. Spence, S.P. Tear, Surf. Sci. 398 (1998) 91.
[5] Y.G. Ding, C.T. Chan and, K.M. Ho, Phys. Rev. Lett. 67 (1991) 1454.
[6] T. Takahashi, S. Nakatani, Surf. Sci. 282 (1993) 17.
[7] D. Jeon, T. Hashizume, T. Sakurai, J. Physique IV 4 (1996) C5–189.
[8] M. Hammar, M. Gothelid, U.O. Karlsson and, S.A. Flodstrom, Phys. Rev. B 47 (1993) 15669.
[9] H.H. Weitering and, J.M. Carpinelli, Surf. Sci. 384 (1997) 240.
[10] C. Collazo-Davila, D. Grozea and, L.D. Marks, Phys. Rev. Lett. 80 (1998) 1678.
[11] L. Lottermoser, E. Landemark, D.-M. Smilgies, M. Nielsen, R. Feidenhans'l, G. Falkenberg, R.L. Johnson, M. Gierer, A.P. Seitsonen, H. Kleine, H. Bludau, H. Over, S.K. Kim, F. Jona, Phys. Rev. Lett. 80 (1998) 3980.
[12] S. Hasegawa, M. Maruyama, Y. Hirata, D. Abe, H. Nakashima, Surf. Sci. 405 (1998) L503.
[13] M. Bertucci, G. Le Lay, M. Manneville and, R. Kern, Surf. Sci. 85 (1979) 471.
[14] G. LeLay, V.Yu. Aristov, L. Seehofer, T. Buslaps, R.L. Johnson, M. Gothelid, M. Hammar, U.O. Karlsson, S.A. Flodstrom, R. Feidenhans'l, M. Nielsen, E. Findeisen and, R.I.G. Uhrberg, Surf. Sci. 307–309 (1994) 280.
[15] M. Göthelid. PhD Thesis; R. Feidenhans'l et al., unpublished data.
[16] M. Woolfson, Fan Hai-fu. Physical and Non-physical Methods of Solving Crystal Structures. Cambridge University Press, Cambridge, 1995.
[17] L.D. Marks and, E. Landree, Acta Cryst. A 54 (1998) 296.
[18] E. Landree, C. Collazo-Davila and, L.D. Marks, Acta Cryst. B 53 (1997) 916.
[19] L.D. Marks, R. Plass, D.L. Dorset, Surf. Rev. Lett. 4 (1997) 1.
[20] C.J. Gilmore, L.D. Marks, D. Grozea, C. Collazo, E. Landree, R.D. Twesten, Surf. Sci. 381 (1997) 77.
[21] C. Collazo-Davila, L.D. Marks, K. Nishii, Y. Tanishiro, Surf. Rev. Lett. 4 (1997) 65.

[22] L.D. Marks, D. Grozea, R. Feidenhans'l, M. Nielsen, R.L. Johnson, Surf. Rev. Lett. 5 (1998) 459.
[23] E. Landree, L.D. Marks, P. Zschack, C.J. Gilmore, Surf. Sci. 408 (1998) 300.
[24] R. Feidenhans'l, Surf. Sci. Rep. 10 (1989) 105.
[25] H. Hauptman, J. Karle. Solution of the Phase Problem. I. The Centrosymmetric Crystal. A.C.A. Monograph No. 3. Edwards Brothers, Inc., Ann Arbor, Michigan, 1953.
[26] L.M. Peng, G. Ren, S.L. Dudarev and, M.J. Whelan, Acta Cryst. A 52 (1996) 456.
[27] S.C. Erwin, H.H. Weitering, Phys. Rev. Lett. 81 (1998) 2296.
[28] R. Plass, L.D. Marks, Surf. Sci. 380 (1997) 497.
[29] K. Higashiyama, S. Kono and, T. Sagawa, Jpn. J. Appl. Phys. 25 (1986) L117.
[30] J. Nogami, A.A. Baski and, C.F. Quate, Phys. Rev. Lett. 65 (1990) 1611.
[31] S. Takahashi, Y. Tanishiro and, K. Takayanagi, Surf. Sci. 242 (1991) 73.
[32] J. Yuhara, M. Inoue and, K. Morita, J. Vac. Sci. Technol. A 10 (1992) 3486.
[33] T. Takami, D. Fukushi, T. Nakayama, M. Uda and, M. Aono, Jpn. J. Appl. Phys. 33 (1994) 3688.
[34] J. Falta, A. Hille, D. Novikov, G. Materlik, L. Seehofer, G. Falkenberg and, R.L. Johnson, Surf. Sci. 330 (1995) L673.
[35] S. Kullback and, R.A. Leibler, Ann. Math. Stat. 22 (1951) 79.
[36] T.M. Cover, J.A. Thomas. Elements of Information Theory. Wiley, New York, 1991.
[37] R.W. Gerchberg, W.O. Saxton, Optik 35 (1972) 237.
[38] J.R. Fienup, Optics Lett. 3 (1978) 27.
[39] J.R. Fienup, J. Optical Soc. Am. 4 (1987) 118.
[40] D. Sayre, Acta Cryst. 5 (1952) 60.